SEISMIC RESPONSE ANALYSIS BY SUBLOADING SURFACE MODEL

KENICHIRO MIYASHITA*, KOICHI HASHIGUCHI†, AND SHIGERU SATO*

* Pacific Consultants Corporation (PCKK)
7-5,Sekido 1-chome, Tama-shi,Tokyo,Japan
Email: kenichirou.miyashita@os.pacific.co.jp - Web page: http://www.pacific.co.jp

† Dept. Dependent and Optimum Design, Joining and Welding Research Institute
Mihogaoka 11-1, Ibaragi-shi, Osaka 567-0047, Japan
Email: khashi@kyudai.jp

Key words: Seismic Response, liquefaction, Elastoplasticity.

1 INTRODUCTION

A lot of disaster by liquefaction have been reported in area along the shore of Japan. In particular, liquefaction has occurred in the wide area in the Great East Japan Earthquake of 2011. Various approaches for the liquefaction analysis have been proposed up to present. Among these approaches, the subloading surface model is formulated in the framework of the plasticity model and thus it is expected to provide a highly pertinent simulation of cyclic loading behaviour of materials. Further, the explicit constitutive equation of soils has been formulated to describe the cyclic loading behaviour with the cyclic mobility [1]. In this study, the validity of the liquefaction analysis by the subloading surface model is examined by comparing the simulation by the subloading surface model with the actual record for the acceleration wave in the ground surface to the input of the actual data of the acceleration wave in the soil ground base. The actual data used in the simulation was recorded in the Kushiro earthquake in 1993. [2]

2 SUBLOADING SURFACE MODEL

Subloading surface model is the elastoplasticity model that considering plastic strain rate induced by the rate of stress inside the yield surface. Its basic concept and equations for subloading surface model is indicated in the following.

2.1 Normal-yield and subloading surfaces

The subloading surface is introduced which always passes through current stress point and has similar shape to the yield surface in subloading surface model, which the yield surface is renamed the *normal-yield surface*. In subloading surface model, the plastic strain rate generates by a change of not only normal-yield surface but also R, which is the ratio of the size of the subloading surface to that of normal-yield surface. R is called as the *normal-yield ratio.* The state R=0 corresponds to the null stress state in which a purely elastic deformation behavior

occurs, the state $0<R<1$ to the subyield state, and the state $R=1$ to the nomal-yield state in which the stress lies on the normal-yield surface for which the plastic strain rate has been formulated in conventional plasticity.The yield surface and the subloading surface are described as Eq.(1) and Eq.(2).

$$f(\boldsymbol{\sigma},\boldsymbol{\beta}) = F(H) \tag{1}$$
$$f(\bar{\boldsymbol{\sigma}},\boldsymbol{\beta}) = RF(H) \tag{2}$$

where

$$\bar{\boldsymbol{\sigma}} \equiv \boldsymbol{\sigma} - \bar{\boldsymbol{\alpha}} \tag{3}$$
$$\bar{\boldsymbol{\alpha}} = (1-R)\boldsymbol{c} \tag{4}$$

$\boldsymbol{\sigma}$ is the Cauchy stress, $\boldsymbol{\beta}$ is the roationl-hardening variable, H is the isotropic hardening variable. $\boldsymbol{c}$ is the elastic-core, i.e the center of similarity of subloading surface to the normal-yield surface. $\bar{\boldsymbol{\alpha}}$ is the similar point in the subloading surface to origin. They are illustrated on the (p,q) plane in Fig.1. where p is mean effective pressure, q is the stress difference between the vertical and horizontal directions.

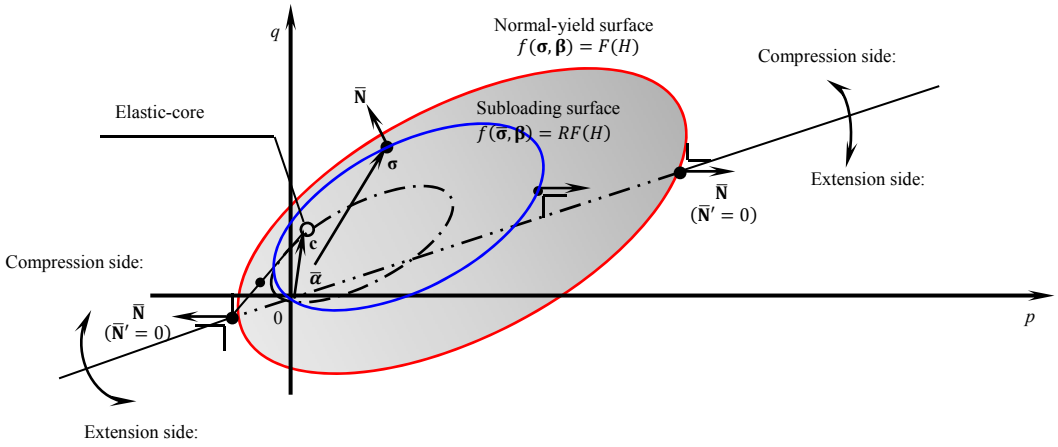

Figure 1: Rotated normal-yield, subloading and similarity-center surfaces in the(p,q)plane

The evolution rule of R is given as Eq.(5), which is based on assumption that as the subloading surface approaches the normal-yield surface, R does not increase gradually , and when the subloading surface corresponds to normal-yield surface, the rate of normal-yield ratio is 1.0.

$$dR = U(R)\|\boldsymbol{D}^{\boldsymbol{p}}\| = \lambda U(R) \tag{5}$$

Where U is monotonically deceasing function of R (See Eq.(6)), $\boldsymbol{D}^{\boldsymbol{p}}$ is plastic strain rate, λ is the magnitude of plastic strain rate. By this modeling, the subloading surface model can express the natural stress-strain curve that the plastic strain rate increase smoothly as stress approaches the normal-yield surface.

$$\left.\begin{aligned} U(R) &= u\cot(\frac{\pi}{2}R) \\ U &= +\infty \text{ for } R = 0 \\ U &= 0 \text{ for } R = 1 \end{aligned}\right\} \tag{6}$$

2.2 The strain rate by the subloading surfaces model

The strain rate by the subloading surface is indicated in the following. The partial derivatives of the Eq.(2) is shown below.

$$\frac{\partial f(\bar{\boldsymbol{\sigma}},\boldsymbol{\beta})}{\partial \bar{\boldsymbol{\sigma}}} : d\boldsymbol{\sigma} - \frac{\partial f(\bar{\boldsymbol{\sigma}},\boldsymbol{\beta})}{\partial \bar{\boldsymbol{\sigma}}} : d\bar{\boldsymbol{\alpha}} + \frac{\partial f(\bar{\boldsymbol{\sigma}},\boldsymbol{\beta})}{\partial \boldsymbol{\beta}} : d\boldsymbol{\beta} = dRF + RdF \tag{7}$$

Eq.(7) is rewritten as below

$$\bar{\boldsymbol{N}} : d\boldsymbol{\sigma} - \bar{\boldsymbol{N}} : \left\{ d\bar{\boldsymbol{\alpha}} + \frac{dF}{F}\bar{\boldsymbol{\sigma}} + \frac{dR}{R}\bar{\boldsymbol{\sigma}} - \frac{1}{RF}\left(\frac{\partial f(\bar{\boldsymbol{\sigma}},\boldsymbol{\beta})}{\partial \boldsymbol{\beta}} : d\boldsymbol{\beta}\right)\bar{\boldsymbol{\sigma}} \right\} = 0 \tag{8}$$

Where

$$\bar{\boldsymbol{N}} \equiv \frac{\partial f(\bar{\boldsymbol{\sigma}},\boldsymbol{\beta})}{\partial \boldsymbol{\sigma}} \Big/ \left\| \frac{\partial f(\bar{\boldsymbol{\sigma}},\boldsymbol{\beta})}{\partial \boldsymbol{\sigma}} \right\| \tag{9}$$

Further, assume the associated flow rule

$$\boldsymbol{D}^{\boldsymbol{p}} = \lambda \bar{\boldsymbol{N}} \tag{10}$$

Let the translation rule of elastic-core and the evolution rule of rotational hardening be given as [1]

$$\mathrm{d}\boldsymbol{c} = \bar{c}\lambda\left(\frac{\bar{\boldsymbol{\sigma}}}{R} - \frac{\boldsymbol{c}}{\chi}\right) + \left(\frac{dF}{F} - \frac{1}{\chi F}\frac{\partial f(\boldsymbol{c},\boldsymbol{\beta})}{\partial \boldsymbol{\beta}} : d\boldsymbol{\beta}\right)\boldsymbol{c} \tag{11}$$

$$\mathrm{d}\boldsymbol{\beta} \equiv \lambda \boldsymbol{b} \tag{12}$$

Where χ , $\bar{c}$ are material parameter. Substituting Eq.(10),Eq.(11),Eq.(12) into Eq.(8) yields

$$\bar{\boldsymbol{N}} : d\boldsymbol{\sigma} - \lambda M^{p} = 0 \tag{13}$$

where

$$M^{p} \equiv \bar{\boldsymbol{N}} : \{\frac{dF}{dH}\frac{h}{F}\bar{\boldsymbol{\sigma}} + \frac{U(R)}{R}(\boldsymbol{\sigma} - \boldsymbol{c}) + \bar{c}(1-R)\left(\frac{\bar{\boldsymbol{\sigma}}}{R} - \frac{\boldsymbol{c}}{\chi}\right) - \frac{1}{RF}\left(\frac{\partial f(\bar{\sigma},\beta)}{\partial \boldsymbol{\beta}} : \boldsymbol{b}\right)\bar{\boldsymbol{\sigma}} - \frac{1-R}{\chi F}\left(\frac{\partial f(\boldsymbol{c},\boldsymbol{\beta})}{\partial \boldsymbol{\beta}} : \boldsymbol{b}\right)\boldsymbol{c}\} \tag{14}$$

$$h \equiv \frac{dH}{\lambda} \tag{15}$$

Then the magnitude of plastic strain rate is given by

$$\lambda = \frac{\bar{\boldsymbol{N}} : d\boldsymbol{\sigma}}{M^{p}} \tag{16}$$

The strain rate is given by

$$\boldsymbol{D} = \boldsymbol{E}^{-1}\!: d\boldsymbol{\sigma} + \lambda \overline{\boldsymbol{N}} \tag{17}$$

Where $\boldsymbol{D}$ is the strain rate, $\boldsymbol{E}$ is young's modulus.

2.3 Description of Cyclic mobility by subloading surface model

Cyclic mobility occurring in the liquefaction in sands is a peculiar phenomenon exhibiting a butterfly-shaped stress loops and a S-shaped stress-strain loops under undrained cyclic loading. In elastoplasticity, Considering the plastic potential different from yield surface, the method that the elastic shear modulus *G* is increased by recovery of the effective pressure is often used as the method of expressing cyclic mobility. However, the physical explanation of the dilatancy is indefinite, because this method considers the 2 kinds of the dilatancy.

The subloading surface model expresses cyclic mobility by formulating the rate of isotropic hardening/softening variable *H* that influence of the deviatoric plastic strain rate is incorporated.

$$h = -tr\overline{N} + \mu_d \left\| \overline{N'} \right\| \frac{\{\frac{\chi_d}{p+\zeta F}\}^a - 1}{\{\frac{\chi_d}{p+\zeta F}\}^{a-1+b}} \tag{18}$$

$$\chi_d \equiv \frac{\|\sigma\prime\|}{M_d} \tag{19}$$

$$M_d \equiv \frac{14\sqrt{6}sin\phi_d}{(3-sin\phi_d)(8+cos3\theta_d)} \tag{20}$$

$$cos3\theta_d \equiv \sqrt{6}tr\boldsymbol{\tau}^3 \tag{21}$$

$$\boldsymbol{\tau} \equiv \frac{\boldsymbol{\sigma'}}{\|\boldsymbol{\sigma'}\|} \tag{22}$$

where μ_d,ϕ_d,a,b and ζ are material constants. The hardening and the softening are induced outside and inside, respectively, conical surface $\|\boldsymbol{\sigma'}\| = M_d(p + \zeta F)$. The deviatoric hardening rate depends nonlinearly on the modified stress ratio $\chi_d/(p + \zeta F)$.

By this method, the subloading surface model is able to express cyclic mobility without considering 2 kinds of the dilatancy. The method of expressing cyclic mobility in detail is indicated in the following.A butterfly-shaped stress-strain loops in cyclic mobility is illustrated in Fig.2(b). This phenomenon can be simulated by subloading surface model as fellows: The deviatoric stress varies under a high effective pressure in the initial stage of cyclic loading so that the plastic volume contraction is induced leading to a denser arrangement of sand particles. To keep the volume constant, elastic volume expansion is induced by the decrease of effective confining pressure under undrained condition. After the effective pressure decreases as represented at the point $\bar{a}$ in Fig.2(c), the deviatoric stress increases over the critical state line by the deviatoric hardening for $\|\boldsymbol{\sigma'}\|/p > tan\phi_d$ and reaches the dense state(tr$\overline{N} > 0$) causing the plastic volume expansion so that the effective pressure increases responding to the elastic volume contraction in order to keep the volume constant.As the dense state with the deviatoric hardening because of $\|\boldsymbol{\sigma'}\|/p > M_c > M_d$ proceeds, the effective stress rise up at almost constant effective stress ratio as represented at the point $\bar{c}$ in Fig.2(c). Consequently, the effective stress path goes up straightly from the origin in the (p,q) plane. The nomal-yield

surface expands markedly so that the strain rate decreases gradually in this process. Then, the $q-\varepsilon_a$ curve gets warped to the upper as shown in this Fig.2(b). where ε_a is the vertical strain.

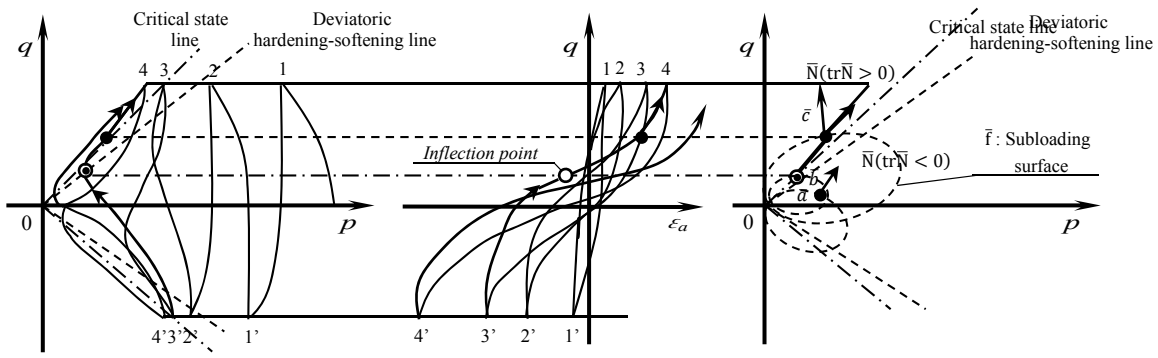

(a)Stess path (b)Stress-strain relation (c) Variations of normal-yield and subloading surfaces

Figure 2: Phenomenon in cyclic mobility

3 THE SIMULATION OF THE KUSHIRO EARTHQUAKE IN 1993

3.1 The acceleration histories of observation

For the Kushiro earthquake, the observation acceleration histories are obtained at ground level GL±0.0 and underground GL -77m at the observation point KUSHIRO G near-shore. KUSHIRO G is a strong-motion observation point managed by a Japanese incorporate administrative agency called the Port and Airport Research Institute, which discloses the observation results on the WEB. Fig. 3 indicates the disclosed wave form observed at KUSHIRO G. The greater acceleration of GL ± 0.0 than of GL -77m indicates that the acceleration was amplified by the resonance with the ground. Also, the wider time interval between peaks of GL±0.0 than of GL -77m, and furthermore, the spike form acceleration wave form after 30 seconds are considered it is caused by the cyclic mobility.

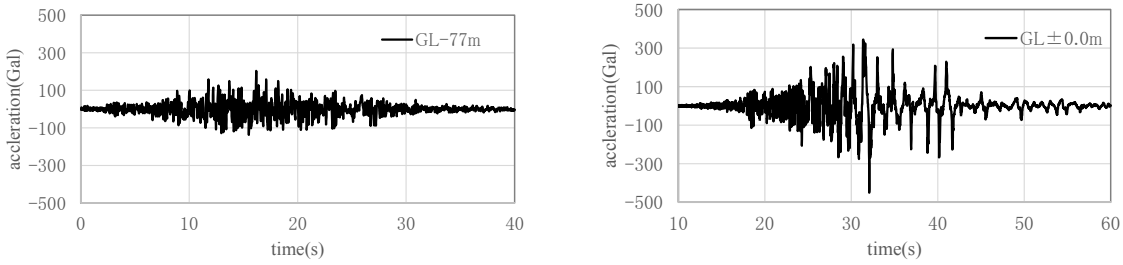

(a)GL-77.0m (a)GL0.0m

Figure 3: Observation acceleration histories

3.2 Ground condition and the material parameters

The speed of s-wave propagation through medium by PS logging and unit weight volume of the ground at observation point KUSHIRO G are also disclosed. The following indicates these values and the material parameters set based on these values.

Table 1: Ground condition and the material parameters

level			layer		ρ (t/m^3)	Vs (m/s)	μ_d	φ_d	a	b	u	c	F_0
0	～	-2	layer1	sand	1.8	146	1	28	3	20	10	20	353
-2	～	-5	layer2	sand	1.8	146	1	28	3	20	10	20	933
-5	～	-13	layer3	sand	1.95	355	1	28	3	20	10	20	1882
-13	～	-24	layer4	sand	1.9	357	1	28	3	20	10	20	3542
-24	～	-37	layer5	sand	2	324	1	28	3	20	10	20	5718
-37	～	-52	layer6	sand	2	324	1	28	3	20	10	20	8383
-52	～	-64	layer7	sand	2	337	1	28	3	20	10	20	10952
-64	～	-77	layer8	sand	2	337	1	28	3	20	10	20	13331

Where F_0 is the parameter of the size of normal-yield surface, V_s is s-wave propagation through medium.

3.3 Simulations of a simple shear test

Prior to run the seismic simulations, simulations of a simple shear test in horizontal direction considering layer2 and 3 shown in the Table 1 were practiced to confirm the reproducibility of the cyclic mobility by the subloading surface model. The stress-strain relationship and stress path obtained by the simulations are shown in Fig. 4. Where, p_c is an initial mean effective pressure, τ_{xz} is a shear stress in horizontal direction, γ_{xz} is a shear strain in horizontal direction. *FLAC3D* based on the explicit dynamic relaxation method is adopted in this simulation.

Fig.4 indicates subloading surface model can well reproduce the cyclic mobility as the stress-strain loops are butterfly-shaped. Also, the stress path well expresses the tracks of mean effective pressures that gradually decrease by the deviatoric stress and then increase linearly in consequence of dilatancy.

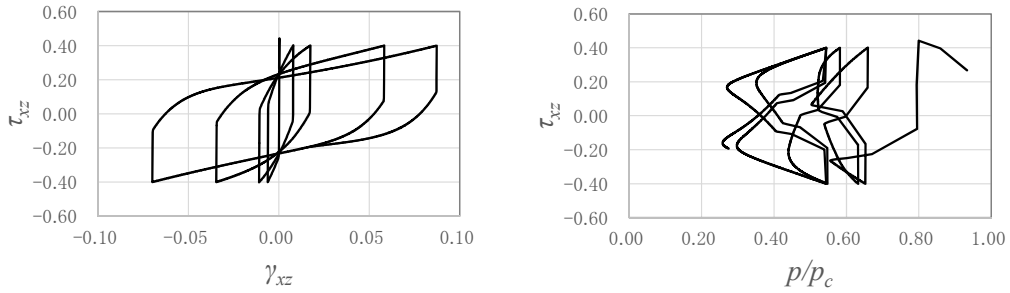

(a)layer2

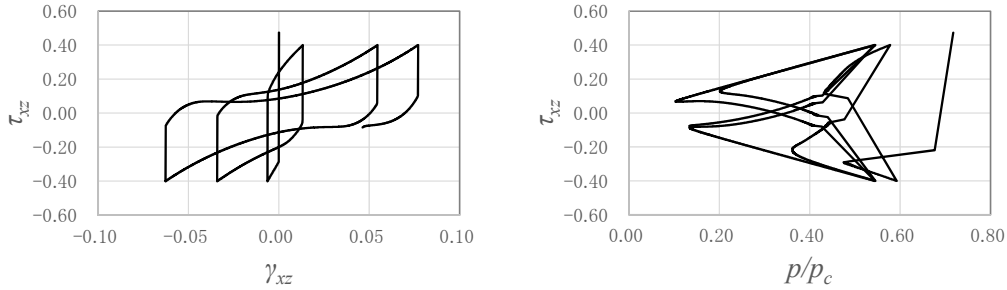

(b)layer3

Figure 4: Simulation of a simple shear test in horizontal direction

3.4 Simulation results

A simulation model was set up considering the horizontal ground between GL±0.0 to GL-77m and run giving the observed wave form at GL-77m.The acceleration history for surface of layer is shown in Fig 5(a). The fourier spectrum of the observed wave form and simulation result is shown in Fig 5(b).

The maximum acceleration obtained by the simulation almost fits the observed data, and the trend that the frequency is prolonged after the occurence of the maximum acceleration is well reproduced. The simulated model shows larger fourier spectrum at higher frequencies compared to the observed wave data, which indicates the model evaluates the ground somewhat harder than the actual situation.

The stress-strain relationship at Layer2 is shown in Fig 6. The cyclic mobility of layer2 is not as explicit as the simple sear test. The observed wave data shows elasticity before the occurence of maximum acceleration, and this study assumed large size of yeilding surface to reproduce the behaviour. It is considered, as the result, the plastic strain became smaller and it disturbed the non-occuremce of the cyclic mobility.

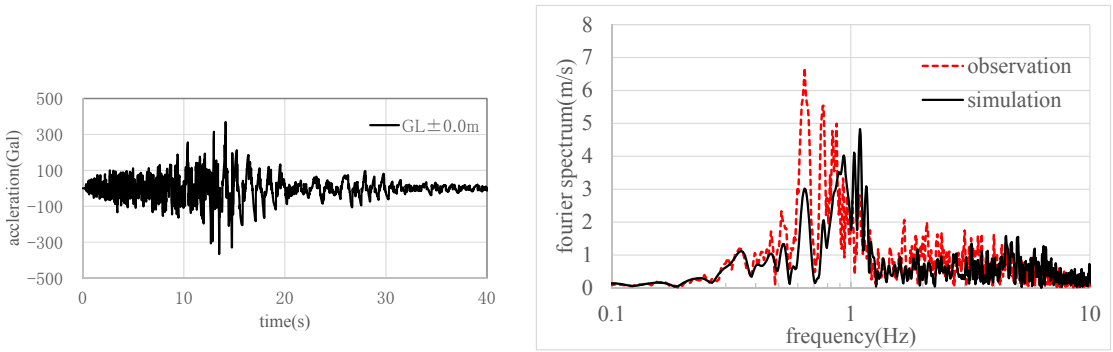

(a)acceleration history for surface (b)fourier spectrum

Figure 5:Results of Simulation

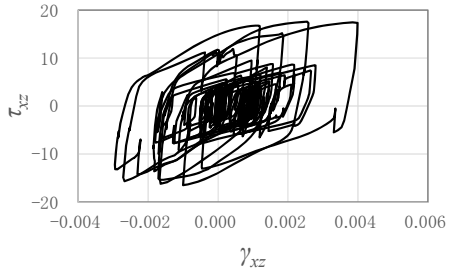

Figure 6:Stress-Strain relationship

4 CONCLUSIONS

- For the simulations of a simple shear test in horizontal direction, the subloading surface model was able to express the cyclic mobility.
- Cyclic mobility of the simulated model was not explicit, but the maximum acceleration obtained by the simulation almost matched the observed data. Also, the trend that the frequency is prolonged after the occurrence of the maximum acceleration was well reproduced.

ACNOWLEDGEMENT

The seismic waves adopted to the study was sourced from an observation point KUSHIRO G installed by a Japanese incorporate administrative agency called the Port and Airport Research Institute.

REFERENCES

[1] K. Hashiguchi, “Elastoplasticity Theory”, Second Edition, Lecture Notes in Applied and Computational Mechanics, Springer (2013).

[2] Strong-motion Seismograph Networks : http:// www. kyoshin. bosai.go.jp /kyoshin/ docs/ kyoshin_index.html